nature structural & molecular biology

Conformational changes required for H^+/Cl^- exchange mediated by a CLC transporter

Daniel Basilio[1], Kristin Noack[1], Alessandra Picollo[1] & Alessio Accardi[1–3]

CLC-type exchangers mediate transmembrane Cl^- transport. Mutations altering their gating properties cause numerous genetic disorders. However, their transport mechanism remains poorly understood. In conventional models, two gates alternatively expose substrates to the intra- or extracellular solutions. A glutamate was identified as the only gate in the CLCs, suggesting that CLCs function by a nonconventional mechanism. Here we show that transport in CLC-ec1, a prokaryotic homolog, is inhibited by cross-links constraining movement of helix O far from the transport pathway. Cross-linked CLC-ec1 adopts a wild-type–like structure, indicating stabilization of a native conformation. Movements of helix O are transduced to the ion pathway via a direct contact between its C terminus and a tyrosine that is a constitutive element of the second gate of CLC transporters. Therefore, the CLC exchangers have two gates that are coupled through conformational rearrangements outside the ion pathway.

The CLC channels and transporters comprise a family of membrane proteins, expressed across a wide variety of organisms, whose primary task is to mediate anion transport[1,2]. The CLCs form dimers, with each monomer delimiting separate Cl^- translocation pathways. These proteins function in two fundamentally different ways: the channels allow rapid and passive anion passage across membranes, and the transporters mediate the stoichiometric exchange of one or two anions for a proton[3–8]. The human genome encodes nine CLC homologs that belong to both functional subtypes, and mutations in at least four CLC genes lead to genetically inherited diseases[1].

Opening of the CLC channels and exchangers is regulated by voltage, H^+ and Cl^- concentrations[1,2], but the conformational changes underlying gating remain poorly understood. High-resolution crystal structures of four CLC transporters have been solved[9–11] but have shed limited mechanistic insight into this process because the transmembrane regions of all four homologs adopt nearly identical conformations (**Fig. 1a**). The only mechanistically telling difference is the position of a highly conserved glutamate side chain, Glu_{ex}, which competes with the Cl^- ions for occupancy of two of the three substrate-binding sites that define the anion transport pathway[11,12]. Upon protonation, Glu_{ex} moves out of the pathway, thereby opening it to the extracellular side (**Fig. 1b**). This, together with extensive functional studies[3,12–15], led to the conclusion that Glu_{ex} is a gate in the CLCs. The lack of other, crystallographically resolved, structural rearrangements led to the hypothesis that movement of Glu_{ex} is the only relevant conformational change occurring during CLC channel and transporter gating[11,12,16]. In support of this minimalistic gating mechanism, functional studies showed that the two subunits function independently[17] and that transport does not require major conformational rearrangements[18,19]. The idea that a single gate regulates ion transport by the CLCs provides a rationale for how the family could have diverged into channels and secondary active transporters, and it explains key features of CLC channel gating. However, a single-gate exchange mechanism is incompatible with the basic tenet of alternating-access transport, which postulates that bound substrates cannot be in simultaneous contact with both sides of the membrane[20]. Indeed, large conformational rearrangements underlie the alternate exposure of substrates to either side of the membrane in most transporters[21–28]. Disruption of these coordinated movements decouples the two gates and can result in channel-like behavior of the transporters, causing the unwanted dissipation of substrate gradients, with potentially catastrophic consequences[29]. A recent attempt to resolve this quandary postulated that in the CLCs the Glu_{ex} gate is assisted by a static kinetic barrier[11,16] possibly formed by the steric constriction of the Cl^- transport pathway at the side chains of conserved residues, Ser107 and Tyr445 in CLC-ec1 (**Fig. 1b**). This static barrier reduces slippage by preventing Cl^- diffusion[11,16] so that, on average, during a protonation-deprotonation event of Glu_{ex} only two Cl^- ions permeate through the 'open' CLC transporter. Kinetic simulations showed that such a mechanism could account for the 2 Cl^-/1 H^+ exchange stoichiometry of the CLCs[11,16]. However, this model fails to explain some of the key functional properties of the CLC transporters, such as the stoichiometry's independence from pH and from the transport rate, the latter of which differs by more than three orders of magnitude among different CLCs[3,10,19]. Furthermore, mutations scattered throughout the transmembrane region strongly affect voltage-dependent gating of CLC channels and transporters[30], in some cases causing genetic disorders. Thus, regions beyond the ion pathway proper might be involved in gating[31,32]. Finally, several lines of evidence suggest that conformational changes in regions distal to

[1]Department of Anesthesiology, Weill Cornell Medical College, New York, New York, USA. [2]Department of Physiology and Biophysics, Weill Cornell Medical College, New York, New York, USA. [3]Department of Biochemistry, Weill Cornell Medical College, New York, New York, USA. Correspondence should be addressed to A.A. (ala2022@med.cornell.edu).

Received 1 September 2013; accepted 26 March 2014; published online 20 April 2014; doi:10.1038/nsmb.2814

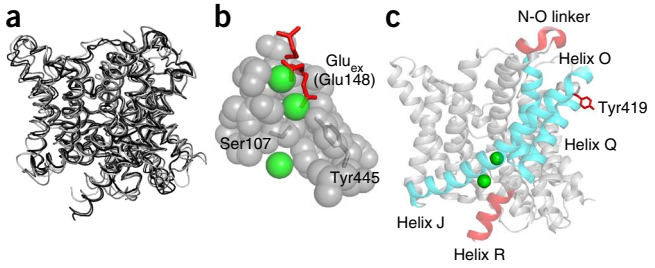

Figure 1 Structural arrangement of CLC-ec1. (**a**) Overlay of the backbone of four CLC homologs: *Escherichia coli* CLC, CLC-ec1 (PDB 1OTS[12], black); *Salmonella enterica* serovar Typhimurium CLC, stCLC (PDB 1KPL[9], dark gray); *Synechocystis* sp. PCC 6803 CLC, cyCLC (PDB 3Q17 (ref. 10), medium gray); and *Cyanidioschyzon merolae* CLC, cmCLC (PDB 3ORG[11], light gray). (**b**) Close up view of the Cl^- binding site of CLC-ec1. Highlighted in red is the side chain of E148. The three conformations are taken from *C. merolae* CLC (down), WT CLC-ec1 (middle) and E148Q CLC-ec1 (up). Cl^- ions are shown as green spheres. (**c**) Ribbon representation of a single subunit of CLC-ec1. Highlighted in red are areas that have been reported to be involved in conformational changes[33–35]. Helices J, O and Q are shown in cyan.

the ion pathway might occur during transport. For example, pH- and Cl^--dependent environmental changes have been reported in helix R[33] and in the P-Q loop at Tyr419 (ref. 34) of CLC-ec1 (**Fig. 1c**), a prokaryotic homolog. Similarly, Zn^{2+} binding to the N-O extracellular loop inhibits the mammalian CLC-4 transporter[35] (**Fig. 1c**). When mapped on the three-dimensional structure of CLC-ec1, these regions delimit a well-defined area (**Fig. 1c**), offering a hint as to what portions of the protein, in addition to the ion pathway, might regulate transport.

We hypothesized that if this region undergoes a conformational rearrangement during the exchange cycle then constraining this motion should inhibit transport. We focused on the helical bundle formed by helices J, O and Q (**Fig. 1c**, cyan), which connect the ion pathway to the three, possibly mobile, regions (**Fig. 1c**, red). To test our hypothesis, we introduced cysteine pairs at their contact points and cross-linked them with divalent Hg^{2+}, a bifunctional thiol-specific reagent[23]. Cross-linking the intracellular portion of helix O to helices Q or J reduced Cl^- transport by 30–100 fold, thus indicating that movement of helix O is required for transport. The cross-linked protein adopted a wild-type (WT)-like conformation, thus showing that the disulfide bond does not distort the structure of the protein. Movement of helix O was transduced to the Cl^- pathway via a direct contact between its C-terminal end and Tyr445. Our results show that transport mediated by CLC-ec1 requires movement of helix O and that Tyr445 forms the inner gate of CLC-ec1.

RESULTS

We conducted our experiments on the background of a well-characterized cysteineless variant of CLC-ec1 that mediates H^+/Cl^- exchange with WT properties[18]. We identified seven points of contact between helices J, O and Q (**Fig. 2a**) and introduced cysteine pairs at these positions, distributed in three regions: external (**Fig. 2b**), central (**Fig. 2c**) and internal (**Fig. 2d**). All double-cysteine mutants, when un–cross-linked, mediated robust Cl^- transport (**Table 1**), with the least active mutant (G259C A399C) being approximately five-fold slower than the WT protein. This reduction was caused by the G259C mutation (**Table 1** and **Supplementary Fig. 1**), whereas the A399C substitution mediated Cl^- transport at WT-like rates (**Table 1** and **Supplementary Fig. 1**). To assess the extent of Hg^{2+}-induced cross-linking, we counted the number of free cysteines by reacting the protein with maleimide–PEG 5000 (mPEG5K) and using a gel shift assay (**Supplementary Figs. 2** and **3**). All cysteine pairs were nearly completely cross-linked after incubation with a four-fold molar excess of Hg^{2+} for ~1 h. PEGylation of the G259C A399C mutant was incomplete even after incubation for 4 h, owing to poor accessibility of the G259C residue to mPEG5K. In the remainder of this work, we will use the Hg subscript to indicate cross-linked mutants, e.g., A399C A432C$_{Hg}$.

Transport requires a rearrangement outside the Cl^- pathway

We assessed the function of the cross-linked proteins and found a striking pattern. Constraining the extracellular portions of helices J, O and Q (**Fig. 2b**) had only modest functional effects. The reduction in transport rate of the cross-linked L252C P424C$_{Hg}$, A392C M425C$_{Hg}$ and A392C T428C$_{Hg}$ mutants was ~30–40% and comparable to that seen for the WT protein after Hg^{2+}-treatment (**Fig. 2e**,**f**, **Supplementary Fig. 4a**,**b** and **Table 1**). This reduction in rate probably reflects a nonspecific effect of Hg^{2+} on the protein. Cross-links in the middle of the transmembrane region, A396C G429C$_{Hg}$ and A396C T428C$_{Hg}$, elicited a moderate reduction, ~30–50% (**Fig. 2g**, **Supplementary Fig. 4c** and **Table 1**). In contrast to these mild effects, constraints placed at the intracellular portions of helices J, O and Q abolished transport almost completely: cross-linking helices O and J (A399C G259C$_{Hg}$) or helices O and Q (A399C

Table 1 Cl^- transport rates of WT and mutant CLC-ec1

Protein	γ (ion s^{-1})	γ_{Hg} (ion s^{-1})	γ_{Hg}/γ	n	n_{Hg}	Cross-linked helices
WT cysteineless	2,337 ± 378	1,341 ± 224	0.57 ± 0.19	6	8	–
L252C P424C	694 ± 77	528 ± 48	0.76 ± 0.15	7	7	J-Q
A392C M425C	1,136 ± 66	753 ± 97	0.66 ± 0.12	7	7	O-Q
A392C T428C	1,734 ± 229	1,177 ± 235	0.68 ± 0.23	7	7	O-Q
A396C T428C	811 ± 96	394 ± 59	0.49 ± 0.13	7	7	O-Q
A396C G429C	714 ± 90	500 ± 77	0.70 ± 0.20	6	4	O-Q
A399C A432C	1,357 ± 87	16 ± 36	0.01 ± 0.03	10	10	O-Q
G259C A399C	552 ± 83	32 ± 19	0.06 ± 0.04	6	6	J-O
A399C A396C	680 ± 26	227 ± 46	0.33 ± 0.08	6	6	O-O
G259C A432C	517 ± 78	320 ± 70	0.62 ± 0.23	15	15	J-Q
A399C A432C E148A Y445A	23,260 ± 1,480	22,255 ± 2,191	0.96 ± 0.16	4	3	O-Q
A399C A432C Y445A	218 ± 37	72 ± 21	0.33 ± 0.15	12	11	O-Q
A399C A432C E148A	564 ± 26	244 ± 21	0.43 ± 0.06	9	9	O-Q
A399C A432C I402G	909 ± 215	572 ± 65	0.63 ± 0.22	6	6	O-Q
A399C A432C I402A	668 ± 57	248 ± 92	0.37 ± 0.17	6	6	O-Q
A399C A432C I402S	967 ± 137	629 ± 54	0.65 ± 0.15	8	8	O-Q
G259C	257 ± 57	–	–	4	–	–
A399C	1,652 ± 160	–	–	3	–	–
A432C	1,268 ± 77	–	–	4	–	–

Cl^- transport rates measured by efflux assay before (γ) and after Hg^{2+} treatment (γ_{Hg}). Reported values are the average ± s.e.m.; n and n_{Hg} are the number of repeats for the untreated and treated mutants respectively, each from at least two independent preparations.

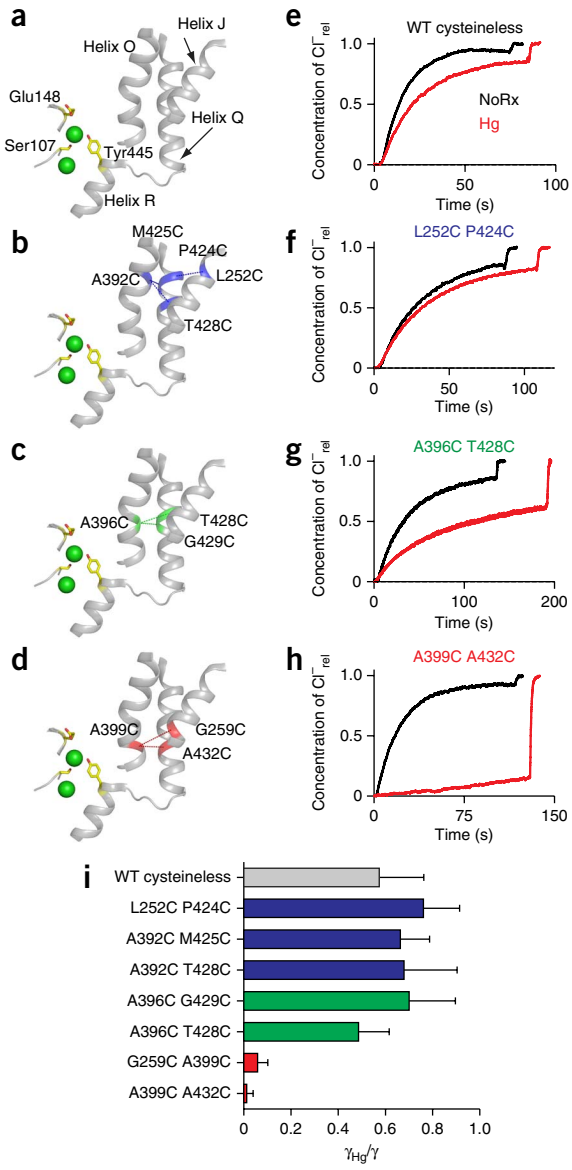

Figure 2 Functional effects of cross-linking helices J, O and Q. (**a**–**d**) Views of the relative position of the Cl^--binding site, helices J, O, Q and R (**a**) and the external (**b**, blue), central (**c**, green) and internal (**d**, red) regions. The positions of the cross-links are indicated by dotted lines. Residues Ser107, Glu148 and Tyr445 are shown as yellow sticks. Cl^- ions are shown as green spheres. (**e**–**h**) Representative time courses of normalized Cl^- efflux from proteoliposomes reconstituted with WT CLC-ec1 (**e**), L252C P424C (**f**), A396C T428C (**g**) or A399C A432C (**h**) mutant CLC-ec1 before (NoRx, black) and after (Hg, red) treatment with Hg^{2+} to induce cross-link formation. For clarity, only traces for one mutant from each group are shown; traces for the other mutants are shown in **Supplementary Figure 4**. (**i**) Average reduction of the transport rate after Hg^{2+}-induced cross-link formation. Bars are color coded as in **a**–**d**. The means ± s.e.m. of the unitary transport rates are shown, and the numbers of repeats are reported in **Table 1**.

$A432C_{Hg}$) reduced transport by ~15-fold and ~100-fold, respectively (**Fig. 2h**, **Supplementary Fig. 4d** and **Table 1**). In the remainder of our work, we used the A399C A432C mutant because, before Hg^{2+} treatment, it has WT-like transport properties, whereas A399C G259C is approximately five-fold slower (**Table 1**). These results (**Fig. 2i**) suggest that during transport the relative movement of the intracellular portions of helices J, O and Q is required for Cl^-/H^+ exchange. Gly259, Ala399 and Ala432 are located far from the binding sites for Cl^- and H^+ (11–22 Å), thus suggesting that cross-linking them does not directly affect the ion pathway and that these residues instead allosterically control ion access to and from the pathway. We then sought to determine what movement is constrained by the cross-links and whether and how it is relayed to the Cl^- pathway.

Structure of the A399C $A432C_{Hg}$ mutant

We crystallized the A399C $A432C_{Hg}$ mutant and solved its structure to 3.5-Å resolution (**Fig. 3a**–**c** and **Table 2**). As expected from our experimental design, the backbone of the A399C $A432C_{Hg}$ mutant superimposes well with that of WT CLC-ec1 (**Fig. 3a**), with an r.m.s. deviation of 0.48 Å. The ion-binding region of the A399C $A432C_{Hg}$ mutant is similar to that of the WT transporter (**Fig. 3b** and **Supplementary Fig. 5a**), with Ser107, Glu148 and Tyr445 occupying their normal positions and with an extra electron density, which we chose to model as a Cl^- atom, given its overlap with the central ion-binding site (**Supplementary Fig. 5a**). Thus, the cross-link does not induce global rearrangements, and the ion pathway is intact.

In the cross-linked protein, helices O and Q are unperturbed (**Fig. 3c**), with the exception of extra electron density bridging them between residues Cys399 and Cys432 (**Fig. 3c** and **Supplementary Fig. 5b**), thus confirming the formation of a cross-link. In an $F_o - F_c$ difference map, the peak intensity of this extra density is ~5σ (**Fig. 3c**), suggesting either low occupancy by Hg^{2+}, which is in contrast to the results seen from the PEGylation experiments (**Supplementary Figs. 2** and **3**) or that Hg^{2+} catalyzed the formation of a disulfide bond between the two cysteines. Therefore, we chose to model this electron density region as a disulfide bond between Cys399 and Cys432 (**Fig. 3c**).

We measured ion binding to the A399C A432C mutant before and after cross-link formation to rule out that subtle distortions of the Cl^- pathway, obfuscated by the limited resolution of our structure, might impair ion binding. The affinity of the unreacted A399C A432C mutant for Cl^- was $K_d \approx 0.9$ mM (**Fig. 3d** and **Supplementary Table 1**), a value similar to that of WT CLC-ec1 (ref. 36). After Hg^{2+} treatment, Cl^- affinity was slightly lowered, to $K_d \approx 3.2$ mM (**Fig. 3e** and **Supplementary Table 1**). This modest effect confirms that the structural integrity of the Cl^- pathway is preserved in the cross-linked protein and supports modeling of the extra electron density in the central binding site with a Cl^- ion (**Fig. 3b**). The ~100-fold reduction of transport in the cross-linked mutant implies that during transport CLC-ec1 adopts a conformation different from that of WT and that this difference involves a rearrangement of helices O and Q.

Helix O moves as a rigid body

The two 'high-impact' cross-links that we identified tether helix O to helix J, G259C $A399C_{Hg}$ (**Supplementary Fig. 4d**) or to helix Q, A399C $A432C_{Hg}$ (**Fig. 2d**,**h**). To determine whether helix O moves relative to J and Q or vice versa, we cross-linked helices J and Q, G259C $A432C_{Hg}$ (**Supplementary Fig. 6a**) and tested whether transport was inhibited. This was not the case: the G259C $A432C_{Hg}$ mutant was less than two-fold slower than its un–cross-linked counterpart (**Supplementary Fig. 6b** and **Table 1**). This, together with the observation that cross-linking helix Q at a nearby position (T433) to the other subunit in the CLC-ec1 dimer does not impair transport[18], suggests that helices J and Q are static while helix O moves.

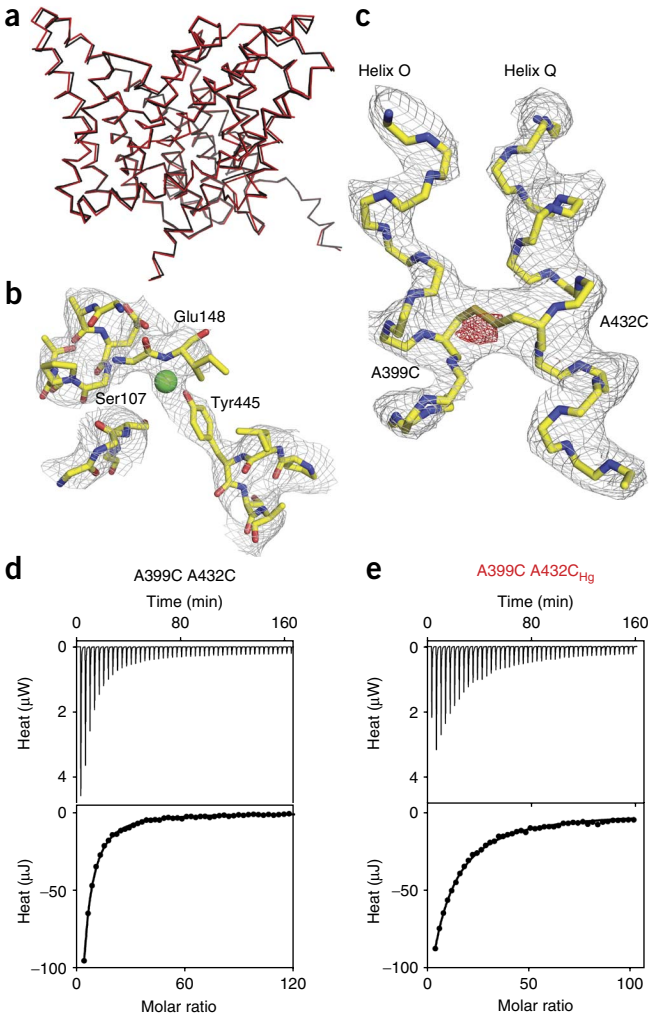

Figure 3 Structure of the A399C A432C cross-linked mutant. (**a**) Overlay of the backbones of WT CLC-ec1 (black, PDB 1OTS[12]) and the A399C A432C$_{Hg}$ mutant (red, PDB 4MQX). (**b**) Structure of the ion-binding region of the A399C A432C$_{Hg}$ mutant. The green sphere represents a Cl^- ion modeled in the central binding site. The electron density is contoured at 1σ. (**c**) Structure of helices O and Q in the A399C A432C$_{Hg}$ mutant. The electron density is contoured at 1.7σ. The $F_o - F_c$ electron density is shown in red and contoured at 3.3σ. (**d**,**e**) Thermograms of Cl^- binding to A399C A432C (**d**) and A399C A432C$_{Hg}$ (**e**). Top graphs show the heats released upon ion binding. Bottom graphs show the integrated heats (circles), and the solid line is the fit to a single-site isotherm. Averaged thermodynamic parameters are reported in **Supplementary Table 1**.

We reasoned that an intrahelix cross-link between Ala396 and Ala399 (**Supplementary Fig. 6c**) might constrain a complex rearrangement of helix O, such as bending or a partial unwinding, whereas a rigid-body motion of the helix (i.e., rotation-translation) should not be affected. The A396C A399C$_{Hg}$ cross-linked mutant was only approximately three-fold slower than the un–cross-linked A396C A399C protein (**Supplementary Fig. 6d** and **Table 1**), suggesting that helix O moves as a rigid body, at least below Ala396.

Movement of helix O is coupled to the Cl^- pathway

To test whether helix O is coupled to the Cl^- pathway, we introduced the A399C A432C$_{Hg}$ cross-link on the background of the channel-like mutant E148A Y445A in which the external gate and internal constriction had been removed[37]. The A399C A432C$_{Hg}$ cross-link had no effect on Cl^- transport mediated by this channelized mutant (**Fig. 4a**, **Table 1** and **Supplementary Fig. 7**), indicating that removal of the Glu148 and Tyr445 side chains decouples Cl^- transport from the conformational cycle of CLC-ec1.

If Glu148 is the only gate (i.e., moving part) regulating Cl^- transport then the A399C A432C$_{Hg}$ cross-link should inhibit transport of the A399C A432C Y445A mutant to the same extent as that seen in the WT protein, because in both constructs the Glu_{ex} gate is intact. This was not the case: transport by the cross-linked Y445A mutant was approximately three-fold slower than that by its unconstrained counterpart, in contrast to the ~100-fold reduction seen with at tyrosine at position 445 (**Fig. 4b**, **Table 1** and **Supplementary Fig. 7**). This result has two implications: first, Glu148 cannot be the only gate regulating Cl^- transport in the CLCs, because the cross-link does not inhibit the A399C A432C Y445A$_{Hg}$ mutant. Second, a second gate exists, and Tyr445 is its critical component.

To determine whether helix O is coupled to only the inner gate through Tyr445 or whether it is also coupled to the outer gate, we tested whether removal of the latter, via the E148A mutation, relieves the inhibitory effect of the cross-link. Transport mediated by the E148A A399C A432C$_{Hg}$ mutant was only ~2.3-fold slower than that by its unreacted counterpart (**Fig. 4c**, **Table 1** and **Supplementary Fig. 7**), suggesting that movement of helix O is not exclusively coupled to the inner gate and rather that movement of this helix regulates Cl^- transport through both gates. Alternatively, the cross-link might act through the H^+ pathway. In this case, the cross-linked protein should be capable of completing a half cycle[38] and therefore of mediating electroneutral Cl^-/Cl^- exchange (**Fig. 4d**). In contrast, if the cross-link affects the Cl^- pathway by 'locking' one or both gates then exchange and net transport should be inhibited to the same extent. Indeed, Cl^-/Cl^- exchange mediated by the A399C A432C$_{Hg}$ mutant was nearly 40-fold slower than that mediated by its un–cross-linked version (**Fig. 4e**). These results suggest that movement of helix O is relayed to the Cl^- pathway and is essential for the coordinated alternate opening of the two gates formed by Glu148 and Tyr445.

Movement of helix O is relayed to the Tyr445 inner gate

In the structures of WT CLC-ec1 and of the cross-linked A399C A432C$_{Hg}$ mutant, the C-terminal residue of helix O, Ile402, sterically interacts with the aromatic ring of Tyr445, a key constituent of the inner gate (**Fig. 5a**). If this interaction is important for coupling helix O to the inner gate then its disruption should have three effects on transport: it should impair turnover, remove the inhibitory effect of the A399C A432C$_{Hg}$ cross-link and alter the transport stoichiometry. Our results met these expectations on all fronts: replacing Ile402 with the smaller side chains glycine, alanine or serine led to an approximately two-fold to four-fold reduction in turnover rate, the A399C A432C$_{Hg}$ cross-link exerted an inhibitory effect of less than two-fold (**Fig. 5b–d**, **Table 1** and **Supplementary Fig. 7**), and the transport stoichiometry of the I402S mutant was degraded by ~50%, to ~3 Cl^-/1 H^+ (**Fig. 6**). These effects are comparable to those caused by mutations of the inner-gate residue Tyr445 on the transport rate, stoichiometry[39,40] and relief of cross-link inhibition (**Fig. 4b**). Thus, the contact between Ile402 and Tyr445 appears to be a key structural element to efficiently transduce movement of helix O to the inner gate and to prevent slippage, suggesting that this interaction is part of the allosteric pathway coupling the two gates of the CLC exchangers. Further work is needed to determine whether additional residues in this region have a role in these processes, for example by coupling helix O to the external gate.

Table 2 Data collection and refinement statistics

	CLC-ec1 cysteineless A399C A432C$_{Hg}$
Data collection	
Space group	*C*2
Cell dimensions	
a, *b*, *c* (Å)	233.5, 94.5, 170.6
α, β, γ (°)	90, 131.75, 90
Resolution (Å)	43.56 (3.52)[a]
R_{merge}	11.5 (52.2)[a]
$I / \sigma I$	6.57 (1.90)[a]
Completeness (%)	98.76 (97.88)[a]
Redundancy	3.3 (3.2)[a]
Refinement	
Resolution (Å)	43.56–3.52
No. reflections	34,345
R_{work} / R_{free}	0.22 / 0.26
No. atoms	
Protein	13,225
Ligand/ion	4
B factors	
Protein	91.5
Ligand/ion	90.9
r.m.s. deviations	
Bond lengths (Å)	0.002
Bond angles (°)	0.620

[a]Values in parentheses are for the highest-resolution shell. Data were collected from a single crystal.

Helix O is coupled to the Cl^- but not the H^+ pathway

Our results cannot rule out the possibility that helix O controls the H^+ pathway in addition to or instead of the Cl^- pathway. We therefore tested whether cross-link formation alters the stoichiometry of transport and thus H^+ coupling. We determined the stoichiometry of transport by simultaneously measuring Cl^- efflux from and H^+ influx into vesicles reconstituted at high protein density (**Fig. 6a**). As expected, the WT protein[3] and the A399C A432C mutant mediated the stoichiometric exchange of two Cl^- ions for one H^+ (**Fig. 6b**,**c**). The A399C A432C I402S and A399C A432C Y445A[39] constructs had degraded transport stoichiometries of ~3 Cl^-/1 H^+ and ~7 Cl^-/1 H^+ (**Fig. 6d**,**e**). All cross-linked mutants mediated exchange with stoichiometries nearly identical to those of the untreated proteins (**Fig. 6c**–**f**). These results are consistent with the hypothesis that helix O is coupled to the Cl^- pathway and that effects on H^+ transport are indirect, if at all present.

DISCUSSION

We set out to test the hypothesis that H^+/Cl^- exchange mediated by the CLC transporters involves conformational rearrangements outside of the Cl^- pathway. We found that we could inhibit transport by constraining movement of the intracellular portion of helix O via covalent cross-links to either helix J or helix Q (**Fig. 2**). A direct interaction between Ile402 and Tyr445 appears to be important in coupling the rearrangement of helix O to the Cl^- pathway, because its disruption impairs turnover, degrades the transport stoichiometry and relieves the inhibitory effect of the A399C A432C$_{Hg}$ cross-link (**Figs. 4**–**6**).

Our results have several notable implications for the exchange mechanism of the CLC transporters. First, the conformational changes occurring during H^+/Cl^- exchange in a CLC transporter involve regions located far from the Cl^- transport pathway. Although several reports previously suggested that this might be the case[33–35], the identification of these conformational rearrangements and the demonstration that they are required for transport was missing. We found that movement of helix O is necessary for transport, because preventing this motion was sufficient to shut down exchange, and that helix O is directly coupled to Tyr445. The conformational rearrangements undergone by helix O during transport are likely to be of limited scope; point mutations disrupting the contact between Ile402 and Tyr445 were sufficient to remove the inhibitory effect of the A399C A432C$_{Hg}$ cross-link (**Figs. 4** and **5**). This conclusion is also consistent with our observation that constraints placed on helix O have graded effects: small on the outside, medium in the center and strong in the internal region (**Fig. 2**). This pattern raises the possibility that only the intracellular half of helix O, below Ala396, moves relative to helices J and Q. A highly conserved glycine residue kinks helix O at position 393 (**Supplementary Fig. 8a**,**b**), just above Ala396, and creates a potentially flexible hinge point separating the mobile intracellular half from the fixed extracellular portion—a scenario that is also compatible with the lack of effect induced by the intrahelix cross-links between Ala396 and Ala399 (**Supplementary Fig. 7**). Alternatively, the cross-links might inhibit a conformational change that is not part of the transport cycle. For example, they might inhibit an active-to-inactive transition, similar to that seen in mammalian CLC channels and exchangers, which involves a concerted rearrangement of both subunits as well as their C termini[41–45]. Although our results cannot rule out this possibility, we think that it is unlikely. Several published lines of evidence suggest that that transport by CLC-ec1 does not entail such a concerted motion, but individual monomers are fully functional[17,18]. Furthermore, in CLC channels mutations at the

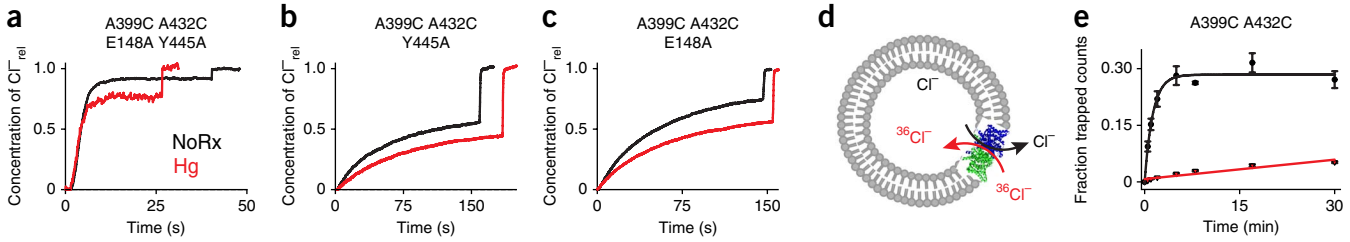

Figure 4 Movement of helix O is coupled to the Cl^- gates. (**a**–**c**) Representative traces of normalized Cl^- efflux mediated by the E148A Y445A (**a**), Y445A (**b**) and E148A (**c**) mutants before (NoRx, black) and after (Hg, red) Hg^{2+}-induced formation of the cross-link at A399C A432C. The average values are reported in **Table 1**. (**d**) Schematic representation of the Cl^- uptake assay. Traces were normalized to the total Cl^- released. (**e**) $^{36}Cl^-$ uptake mediated by the A399C A432C mutant before (black circles, $n = 3$) and after (red triangles, $n = 6$) Hg^{2+}-induced cross-link formation. Symbols are the average ± s.e.m. of n time points. Solid lines represent the fits to a rising exponential (for A399C A432C) of the form $C(t) = a_M \times (1 - \exp(-t/\tau))$, with $a_M = 0.28 \pm 0.08$ and $\tau = 0.77 \pm 0.09$ min^{-1} for an initial rate K for A399C A432C = 0.22 ± 0.06 min^{-1}. The data for the cross-linked A399C A432C$_{Hg}$ were fit to a line of the form $a_0 + Kt$ with $a_0 = 0.007 \pm 0.03$ and K for A399C A432C$_{Hg}$ = 0.0017 ± 0.0002 min^{-1}. The errors on the fitted values represent the uncertainty on the fit.

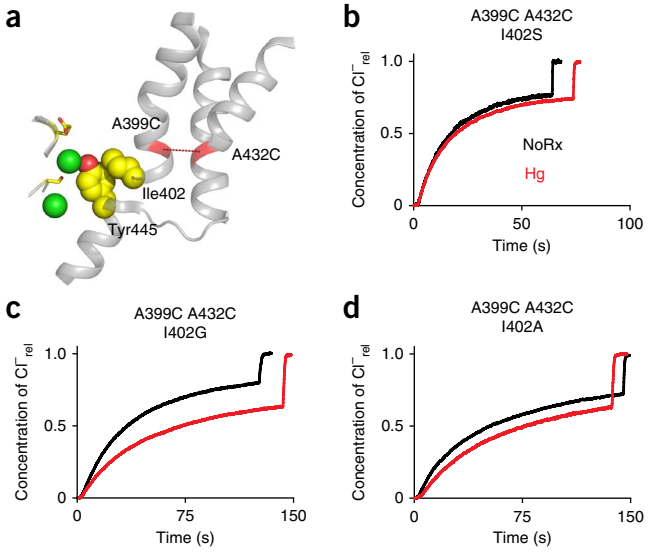

Figure 5 I402 couples helix O to Y445. (**a**) View of the relative position of the Cl^--binding site, helices J, O, Q and R, the A399C A432C cross-link (red dotted line) and the Ile402 Tyr445 contact (yellow, space-filling representation). The gating residues Ser107 and Glu148 are shown as yellow sticks. Cl^- ions are shown as green spheres. (**b**–**d**) Representative traces of Cl^- efflux mediated by the I402S (**b**), I402G (**c**) and I402A (**d**) mutants on the background of the A399C A432C mutant before (black traces) and after (red traces) formation of the cross-link. The average values and number of repeats are reported in **Table 1**.

tyrosine corresponding to Tyr445 dramatically affect this concerted transition[46], whereas similar mutations in CLC-ec1 have minor effects on turnover[40], results consistent with the idea that transport by this homolog does not entail such a transition.

The second major implication of our results is that the CLC transporters have two gates: Glu148 is the external gate, and Tyr445 is a key element of the internal one. If Glu148 were the only gate regulating CLC transport then movements of helix O should affect the Cl^- pathway through this residue alone. In contrast, we found that the movement of helix O is transduced to the Cl^- pathway via a direct interaction between Ile402 and Tyr445 and that the Y445A mutant is also sufficient to remove the inhibitory effects of the cross-link. How movement of helix O, by consequence of Tyr445, is coupled to the external gate remains to be elucidated. Two possibilities that are not mutually exclusive come to mind. The most parsimonious explanation is that the permeant ions themselves couple the two gates by a mixture of steric and electrostatic interactions within the narrow confines of the Cl^- transport pathway. This would explain how maneuvers lowering the ion pathway's affinity for ions degrade transport coupling[39,40,47]. Alternatively, helix O might be coupled to the external gate through the complex network of helices forming the CLC topology, for example via a contact with helix N. This would explain how mutations of residues far from the ion pathway can cause diseases by severely affecting gating and voltage dependence of CLC channels and transporters[31,45,48–50] or transport inhibition caused by Zn^{2+} binding to the N-O loop of CLC-4 (ref. 35). These possibilities are not mutually exclusive; the inner and outer gates could be coupled through both the ion pathway and the protein. This dual mechanism could allow evolution to fine-tune the gating of the CLC channels and transporters to fit diverse physiological roles that range from controlling acidification in intracellular compartments to muscle contraction and salt reabsorption in the kidney. Further work is needed to elucidate the coupling mechanism between the inner and outer gates in the CLC transporters.

A transport model for the CLC exchangers

Our findings, together with previous work, allow us to propose a new model describing the CLC exchange cycle (**Fig. 7**). The experimental observations built into our proposal are: (i) the transport stoichiometry is 2 Cl^-/1 H^+ (ref. 3); (ii) Glu148 adopts three distinct conformations[9,11,12]; (iii) Glu148 and Tyr445 respectively form the external[12]

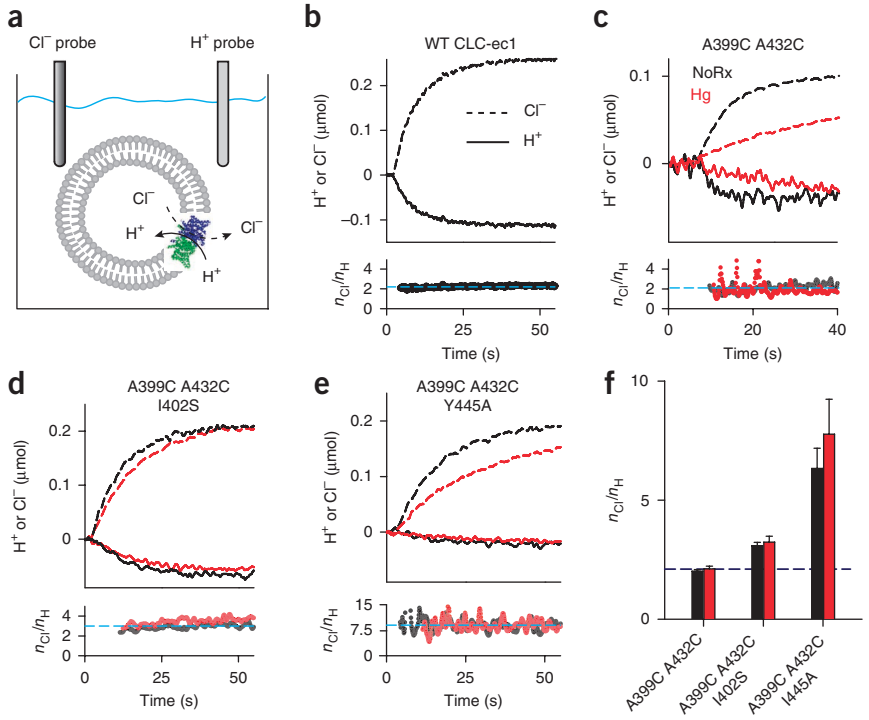

Figure 6 Effects of cross-linking helix O on the Cl^-/H^+ exchange stoichiometry. (**a**) Schematic representation of the simultaneous Cl^- and H^+ flux recordings. (**b**–**e**) Top, simultaneous recordings of Cl^- efflux into (dashed lines) and H^+ efflux from (solid lines) proteoliposomes reconstituted with WT CLC-ec1 (**b**), A399C A432C (**c**), A399C A432C I402S (**d**) or A399C A432C Y445A (**e**) before (black traces) and after (red traces) formation of the cross-link. Bottom, time course of the stoichiometry of transport determined as the ratio of the total transported Cl^- and H^+ ions (n_{Cl}/n_H). Dashed cyan line indicates the average value for the traces shown. (**f**) Average stoichiometry of transport for the A399C A432C (n_{Cl}/n_H(NoRx) = 2.0 ± 0.1, n = 5; n_{Cl}/n_H(Hg) = 2.1 ± 0.1, n = 8), A399C A432C I402S (n_{Cl}/n_H(NoRx) = 3.1 ± 0.1, n = 7; n_{Cl}/n_H(Hg) = 3.2 ± 0.2, n = 8) and A399C A432C Y445A (n_{Cl}/n_H(NoRx) = 6.3 ± 0.8, n = 5; n_{Cl}/n_H(Hg) = 7.8 ± 1.4, n = 4) mutants before (black bars) and after (red bars) Hg treatment. The dashed blue line indicates the WT value (n_{Cl}/n_H = 2.2 ± 0.1, n = 5). Data are shown as average ± s.e.m. of n experiments from two or more independent preparations.

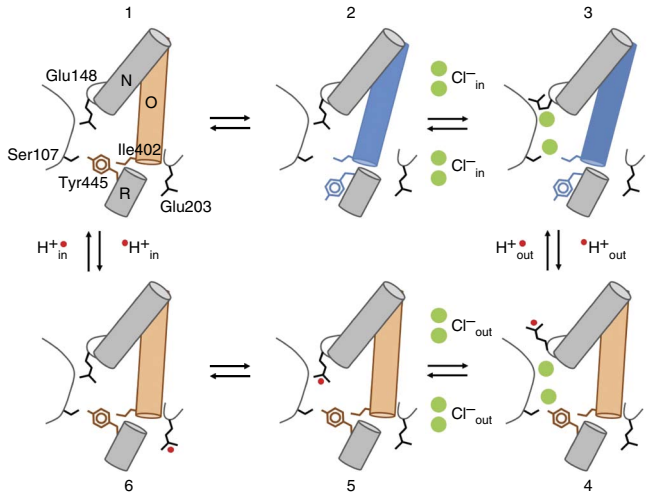

Figure 7 Transport cycle for Cl^-/H^+ exchange in the CLC transporters. The details of the transport model are given in the main text. The initial state is the apo state with the inner (Tyr445) and outer (Glu148) gates closed (1). The inner gate opens (2), thereby allowing Cl^- binding to CLC-ec1 (3). The inner gate closes, and the external gate opens and becomes protonated (4). Cl^- ions can move to the extracellular solution, and the external gate closes while still protonated (5). The proton goes to the intracellular proton acceptor, Glu203 and subsequently diffuses into the intracellular solution, thus returning the transporter to the apo state (6).

and internal gates (**Fig. 5**); (iv) opening of the two gates is coupled through helix O (**Fig. 6**); (v) Cl^- and H^+ binding is synergistic[38]; and (vi) proton exchange with the intracellular solution occurs via Glu203 (ref. 51). A conformational change to the transporter in its apo and occluded state (state 1) opens the inner gate to allow two Cl^- ions to bind from the intracellular side (state 2). This binding causes Glu148's displacement (state 3) as well as its protonation from the outside and triggers the closure of the inner gate. This gives rise to a fully loaded state of the transporter in its outward-facing conformation (state 4). A closed intracellular gate guarantees that the Cl^- ions will exit to the extracellular solution. The still-protonated Glu148 then reenters the ion-transport pathway (state 5), and the proton from Glu148 is somehow transferred to Glu203 (state 6) to be released toward the intracellular solution (state 1). Every step in the proposed cycle (**Fig. 7**) is reversible and does not require additional *ad hoc* assumptions to describe H^+/Cl^- exchange by the CLCs. The synergistic binding of the substrates gives rise to a fully loaded state in which two Cl^- ions and one H^+ are simultaneously bound to the transporter[38] (**Fig. 7d**), a state that is explicitly forbidden for classical 'ping-pong' alternating-access exchange mechanisms. Our data suggest that helix O is part of the coupling machinery between the two gates, and we hypothesize that this allows the simultaneous binding of substrates to occur while preventing ion slippage. Finally, the mechanism leading to opening of the inner gate in the apo state (**Fig. 7a**,**b**) cannot be inferred from known data, and the structure of the ion-free CLC-ec1 is similar to that of the ion-bound form[52]. It is possible that the two states might exist in thermal equilibrium that is shifted toward state 3 by Cl^- binding. We hypothesize, on the basis of our finding that the A399C A432C_{Hg} cross-link inhibits Cl^-/Cl^- exchange as well as net Cl^- transport (**Figs. 2** and **5**), that it prevents the transition between either states 1 and 2 or states 3 and 4. This proposed cycle also explains other, more unusual, characteristics of the CLC transporters. For example, the direct correlation between the size of the side chain at the inner-gate position 445 and the stoichiometry of transport[39,40] is easily rationalized, because smaller residues do not efficiently seal the intracellular access of the pathway, so that state 4 becomes leaky to Cl^- and therefore degrades coupling. Similarly, the presence of a pH-independent inner gate enables the CLC exchangers to sustain tight coupling even at acidic pHs, a necessity in light of their role in survival of enteric bacteria under the extreme acid challenges presented by the host's stomach[53]. The CLC channels might have originated because of mutations that led to the disruption of the seal formed by the inner gate. This predicts that remnants of the CLC exchange cycle should remain in the gating of the CLC channels. Indeed, the key role of Glu_{ex} in CLC channel gating is well documented[12,54] and, in at least one case, channel gating entails transmembrane H^+ transport[55]. Finally, in the CLC-0 and CLC-1 channels[56] Thr471 and Ser537, which correspond to Ile402 in CLC-ec1, selectively affect the apparent affinity of blockers for the closed but not the open state, suggesting that gating in these homologs entails a conformational change likely to involve their intracellular vestibules[56]. Our results suggest that the conformational rearrangements of helix O might be evolutionarily conserved in the gating processes of both CLC channels and transporters. Further work is needed to elucidate how these movements lead to the coordinated opening and closing of the inner and outer gates of the CLC transporters yet how in the CLC channels movement of the outer gate is sufficient to allow for ion permeation. Elucidating the conformational changes underlying gating of the CLC channels and transporters may allow researchers to understand how disease-causing mutations disrupt the function of these proteins and may enable design of new therapies for these devastating conditions.

METHODS

Methods and any associated references are available in the online version of the paper.

Accession codes. Coordinates and structure factors for the Hg^{2+}-treated A399C A432C mutant of CLC-ec1 has been deposited in the Protein Data Bank under accession number 4MQX.

Note: Any Supplementary Information and Source Data files are available in the online version of the paper.

ACKNOWLEDGMENTS

The authors wish to thank C. Miller (Brandeis University) for the generous gift of ^{36}Cl and O. Boudker, C. Nimigean, O. Andersen and members of the Accardi laboratory for helpful discussions and comments on the manuscript. This work was supported by US National Institutes of Health grant GM085232 and an Irma T. Hirschl–Monique Weill-Caulier Scholar Award (to A.A.).

AUTHOR CONTRIBUTIONS

D.B., K.N. and A.P. performed experiments; D.B. and A.A. analyzed the data; A.A. designed research and wrote the paper; and all authors contributed to the editing of the manuscript.

COMPETING FINANCIAL INTERESTS

The authors declare no competing financial interests.

1. Jentsch, T.J. CLC chloride channels and transporters: from genes to protein structure, pathology and physiology. *Crit. Rev. Biochem. Mol. Biol.* **43**, 3–36 (2008).
2. Accardi, A. & Picollo, A. CLC channels and transporters: proteins with borderline personalities. *Biochim. Biophys. Acta* **1798**, 1457–1464 (2010).
3. Accardi, A. & Miller, C. Secondary active transport mediated by a prokaryotic homologue of CIC Cl^- channels. *Nature* **427**, 803–807 (2004).
4. Picollo, A. & Pusch, M. Chloride/proton antiporter activity of mammalian CLC proteins CIC-4 and CIC-5. *Nature* **436**, 420–423 (2005).

5. Scheel, O., Zdebik, A.A., Lourdel, S. & Jentsch, T.J. Voltage-dependent electrogenic chloride/proton exchange by endosomal CLC proteins. *Nature* **436**, 424–427 (2005).
6. Graves, A.R., Curran, P.K., Smith, C.L. & Mindell, J.A. The Cl-/H+ antiporter ClC-7 is the primary chloride permeation pathway in lysosomes. *Nature* **453**, 788–792 (2008).
7. De Angeli, A. *et al.* The nitrate/proton antiporter AtCLCa mediates nitrate accumulation in plant vacuoles. *Nature* **442**, 939–942 (2006).
8. Stockbridge, R.B. *et al.* Fluoride resistance and transport by riboswitch-controlled CLC antiporters. *Proc. Natl. Acad. Sci. USA* **109**, 15289–15294 (2012).
9. Dutzler, R., Campbell, E.B., Cadene, M., Chait, B.T. & MacKinnon, R. X-ray structure of a ClC chloride channel at 3.0 Å reveals the molecular basis of anion selectivity. *Nature* **415**, 287–294 (2002).
10. Jayaram, H., Robertson, J.L., Wu, F., Williams, C. & Miller, C. Structure of a slow CLC Cl^-/H^+ antiporter from a cyanobacterium. *Biochemistry* **50**, 788–794 (2011).
11. Feng, L., Campbell, E.B., Hsiung, Y. & MacKinnon, R. Structure of a eukaryotic CLC transporter defines an intermediate state in the transport cycle. *Science* **330**, 635–641 (2010).
12. Dutzler, R., Campbell, E.B. & MacKinnon, R. Gating the selectivity filter in ClC chloride channels. *Science* **300**, 108–112 (2003).
13. Chen, T.Y., Chen, M.F. & Lin, C.W. Electrostatic control and chloride regulation of the fast gating of ClC-0 chloride channels. *J. Gen. Physiol.* **122**, 641–651 (2003).
14. Zúñiga, L. *et al.* The voltage-dependent ClC-2 chloride channel has a dual gating mechanism. *J. Physiol. (Lond.)* **555**, 671–682 (2004).
15. Engh, A.M., Faraldo-Gomez, J.D. & Maduke, M. The mechanism of fast-gate opening in ClC-0. *J. Gen. Physiol.* **130**, 335–349 (2007).
16. Feng, L., Campbell, E.B. & MacKinnon, R. Molecular mechanism of proton transport in CLC Cl^-/H^+ exchange transporters. *Proc. Natl. Acad. Sci. USA* **109**, 11699–11704 (2012).
17. Robertson, J.L., Kolmakova-Partensky, L. & Miller, C. Design, function and structure of a monomeric ClC transporter. *Nature* **468**, 844–847 (2010).
18. Nguitragool, W. & Miller, C. CLC Cl^-/H^+ transporters constrained by covalent cross-linking. *Proc. Natl. Acad. Sci. USA* **104**, 20659–20665 (2007).
19. Zdebik, A.A. *et al.* Determinants of anion-proton coupling in mammalian endosomal CLC proteins. *J. Biol. Chem.* **283**, 4219–4227 (2008).
20. Jardetzky, O. Simple allosteric model for membrane pumps. *Nature* **211**, 969–970 (1966).
21. Morth, J.P. *et al.* Crystal structure of the sodium-potassium pump. *Nature* **450**, 1043–1049 (2007).
22. Olesen, C. *et al.* The structural basis of calcium transport by the calcium pump. *Nature* **450**, 1036–1042 (2007).
23. Reyes, N., Ginter, C. & Boudker, O. Transport mechanism of a bacterial homologue of glutamate transporters. *Nature* **462**, 880–885 (2009).
24. Kaback, H.R., Smirnova, I., Kasho, V., Nie, Y. & Zhou, Y. The alternating access transport mechanism in LacY. *J. Membr. Biol.* **239**, 85–93 (2011).
25. Forrest, L.R., Krämer, R. & Ziegler, C. The structural basis of secondary active transport mechanisms. *Biochim. Biophys. Acta* **1807**, 167–188 (2011).
26. Perez, C., Koshy, C., Yildiz, O. & Ziegler, C. Alternating-access mechanism in conformationally asymmetric trimers of the betaine transporter BetP. *Nature* **490**, 126–130 (2012).
27. Krishnamurthy, H. & Gouaux, E. X-ray structures of LeuT in substrate-free outward-open and apo inward-open states. *Nature* **481**, 469–474 (2012).
28. Shi, Y. Common folds and transport mechanisms of secondary active transporters. *Annu. Rev. Biophys.* **42**, 51–72 (2013).
29. Artigas, P. & Gadsby, D.C. Na^+/K^+-pump ligands modulate gating of palytoxin-induced ion channels. *Proc. Natl. Acad. Sci. USA* **100**, 501–505 (2003).
30. Ludewig, U., Jentsch, T.J. & Pusch, M. Analysis of a protein region involved in permeation and gating of the voltage-gated *Torpedo* chloride channel ClC-0. *J. Physiol. (Lond.)* **498**, 691–702 (1997).
31. Pusch, M., Steinmeyer, K., Koch, M.C. & Jentsch, T.J. Mutations in dominant human myotonia congenita drastically alter the voltage dependence of the CIC-1 chloride channel. *Neuron* **15**, 1455–1463 (1995).
32. Pusch, M. Myotonia caused by mutations in the muscle chloride channel gene CLCN1. *Hum. Mutat.* **19**, 423–434 (2002).
33. Bell, S.P., Curran, P.K., Choi, S. & Mindell, J.A. Site-directed fluorescence studies of a prokaryotic ClC antiporter. *Biochemistry* **45**, 6773–6782 (2006).
34. Elvington, S.M., Liu, C. & Maduke, M. Substrate-driven conformational changes in ClC-ec1 observed by fluorine NMR. *EMBO J.* **28**, 3090–3102 (2009).
35. Osteen, J.D. & Mindell, J.A. $Zn2^+$ inhibition of CLC-4. *Biophys. J.* **95**, 4668–4675 (2008).
36. Picollo, A., Malvezzi, M., Houtman, J.C. & Accardi, A. Basis of substrate binding and conservation of selectivity in the CLC family of channels and transporters. *Nat. Struct. Mol. Biol.* **16**, 1294–1301 (2009).
37. Jayaram, H., Accardi, A., Wu, F., Williams, C. & Miller, C. Ion permeation through a Cl^- selective channel designed from a CLC Cl^-/H^+ exchanger. *Proc. Natl. Acad. Sci. USA* **105**, 11194–11199 (2008).
38. Picollo, A., Xu, Y., Johner, N., Bernèche, S. & Accardi, A. Synergistic substrate binding determines the stoichiometry of transport of a prokaryotic H^+/Cl^- exchanger. *Nat. Struct. Mol. Biol.* **19**, 525–531 (2012).
39. Accardi, A., Lobet, S., Williams, C., Miller, C. & Dutzler, R. Synergism between halide binding and proton transport in a CLC-type exchanger. *J. Mol. Biol.* **362**, 691–699 (2006).
40. Walden, M. *et al.* Uncoupling and turnover in a Cl^-/H^+ exchange transporter. *J. Gen. Physiol.* **129**, 317–329 (2007).
41. Bykova, E.A., Zhang, X.D., Chen, T.Y. & Zheng, J. Large movement in the C terminus of CLC-0 chloride channel during slow gating. *Nat. Struct. Mol. Biol.* **13**, 1115–1119 (2006).
42. Zifarelli, G. & Pusch, M. Intracellular regulation of human ClC-5 by adenine nucleotides. *EMBO Rep.* **10**, 1111–1116 (2009).
43. De Angeli, A. *et al.* ATP binding to the C terminus of the *Arabidopsis thaliana* nitrate/proton antiporter, AtCLCa, regulates nitrate transport into plant vacuoles. *J. Biol. Chem.* **284**, 26526–26532 (2009).
44. Orhan, G., Fahlke, C. & Alekov, A.K. Anion- and proton-dependent gating of ClC-4 anion/proton transporter under uncoupling conditions. *Biophys. J.* **100**, 1233–1241 (2011).
45. Leisle, L., Ludwig, C.F., Wagner, F.A., Jentsch, T.J. & Stauber, T. ClC-7 is a slowly voltage-gated $2Cl^-/1H^+$-exchanger and requires Ostm1 for transport activity. *EMBO J.* **30**, 2140–2152 (2011).
46. Bennetts, B. & Parker, M.W. Molecular determinants of common gating of a ClC chloride channel. *Nat. Commun.* **4**, 2507 (2013).
47. Nguitragool, W. & Miller, C. Uncoupling of a CLC Cl^-/H^+ exchange transporter by polyatomic anions. *J. Mol. Biol.* **362**, 682–690 (2006).
48. Ludewig, U., Jentsch, T.J. & Pusch, M. Inward rectification in ClC-0 chloride channels caused by mutations in several protein regions. *J. Gen. Physiol.* **110**, 165–171 (1997).
49. Wollnik, B., Kubisch, C., Steinmeyer, K. & Pusch, M. Identification of functionally important regions of the muscular chloride channel CIC-1 by analysis of recessive and dominant myotonic mutations. *Hum. Mol. Genet.* **6**, 805–811 (1997).
50. Saviane, C., Conti, F. & Pusch, M. The muscle chloride channel CIC-1 has a double-barreled appearance that is differentially affected in dominant and recessive myotonia. *J. Gen. Physiol.* **113**, 457–468 (1999).
51. Accardi, A. *et al.* Separate ion pathways in a Cl^-/H^+ exchanger. *J. Gen. Physiol.* **126**, 563–570 (2005).
52. Lobet, S. & Dutzler, R. Ion-binding properties of the ClC chloride selectivity filter. *EMBO J.* **25**, 24–33 (2006).
53. Iyer, R., Iverson, T.M., Accardi, A. & Miller, C. A biological role for prokaryotic ClC chloride channels. *Nature* **419**, 715–718 (2002).
54. Traverso, S., Elia, L. & Pusch, M. Gating competence of constitutively open CLC-0 mutants revealed by the interaction with a small organic inhibitor. *J. Gen. Physiol.* **122**, 295–306 (2003).
55. Lísal, J. & Maduke, M. The ClC-0 chloride channel is a 'broken' Cl^-/H^+ antiporter. *Nat. Struct. Mol. Biol.* **15**, 805–810 (2008).
56. Accardi, A. & Pusch, M. Conformational changes in the pore of CLC-0. *J. Gen. Physiol.* **122**, 277–293 (2003).

ONLINE METHODS

Protein purification. Expression and purification of WT and mutant CLC-ec1 was performed according to the published protocols[39,51,57]. In some preparations the detergent was exchanged from 5 mM DM (*n*-decyl-β-D-maltopyranoside) to 1 mM DMNG (2,2-dioctylpropane-1,3-bis-β-D-maltopyranoside). The protein remains stable in both detergents. The eluted protein was run on a Superdex 200 column (GE Healthcare) preequilibrated in 100 mM NaCl, 20 mM HEPES, 5 mM DM or 50 μM DMNG, pH 7.5 (buffer B), for liposome reconstitution and crystallography.

Mercury-induced cross-link and PEGylation assay. After purification, the protein sample reacted with a four-fold molar-ratio excess of $HgCl_2$ for 1 h at room temperature. Excess Hg^{2+} was removed by addition of 1 mM EDTA and/or gel filtration. Successive reruns of the purified protein showed that it remained stable. To determine whether the introduced cysteines become cross-linked after incubation with Hg^{2+}, we used a gel shift assay (**Supplementary Fig. 2**). The purified protein was concentrated to ~1 mg/ml, and 3 μl of 40 mM maleimide 5,000 PEG (mPEG5K; Sigma-Aldrich) was added to 20 μl of Hg-reacted and unreacted protein samples in the presence of 0.5% sodium dodecyl sulfate (SDS) to unfold the protein. Over time, single cysteine mutants shift from their unreacted position to a single band of higher molecular weight (MW) (**Supplementary Fig. 2a**), whereas the double mutants eventually convert to a second band of higher MW that corresponds to a doubly reacted protein (**Supplementary Fig. 2b**). The reaction of the protein with mPEG5K is completely prevented by incubation with a four-fold molar excess of Hg^{2+} for 60 min (**Supplementary Fig. 2c**), thus indicating that Hg^{2+} oxidizes the cysteines. Furthermore, a 1:1 molar ratio of Hg^{2+} to protein is sufficient to protect both cysteines present in two different double mutants, A399C A432C and A392C T428C (**Supplementary Fig. 2d**,**e**), thus suggesting that Hg^{2+} induces the formation of a cross-link. In all cases the proteins ran mostly as monodisperse peaks on gel filtration after cross-link formation (**Supplementary Fig. 2f**), thus indicating that the Hg treatment was well tolerated. A 60-min incubation with Hg^{2+} was sufficient to completely cross-link all seven double mutants (**Supplementary Fig. 3**).

Liposome reconstitution. *E. coli* polar lipids (Avanti lipids) were dried under N_2 and resuspended in pentane and dried again. The dry lipids were suspended to a final concentration of 20 mg/ml in reconstitution buffer (buffer R) 300 mM KCl, 25 mM citric acid and adjusted to pH 4.5 with NaOH, to which 35 mM 3-[(3-cholamidopropyl)dimethylammonio]-1-propanesulfonate (CHAPS) was added. The suspension was bath sonicated to clarity, and after a 2-h incubation the purified protein was added to the desired concentration: 0.2–1 μg protein/mg lipid for proteoliposome reconstitution and 1.5 μg/mg for $^{36}Cl^-$ uptake. Detergent was dialyzed out overnight in buffer R, and the resulting liposomes were flash frozen in ethanol/dry ice and stored at −80 °C.

Measurement of Cl^- and H^+ fluxes and rate determination. H^+ and Cl^- efflux measurements were carried out as described[3,40]. Briefly, H^+ influx and Cl^- efflux (as indicated) were initiated by the addition of 1 μl of 1 mg/ml of the K^+ ionophore valinomycin, which has a dual role: it shunts the voltage established by the Cl^- gradient and sets the membrane potential to the K^+ equilibrium potential. The time courses of H^+ and Cl^- fluxes were respectively monitored with a pH meter or an Ag/AgCl electrode. H^+ influx was terminated by the addition of 1 μl of 1 mg/ml of the H^+ ionophore carbonyl cyanide 4-(trifluoromethoxy)phenylhydrazone (FCCP), and Cl^- efflux was terminated by the addition of 40 μl of 1.5 M *n*-octyl-β-D-glucopyranoside (Affymetrix) to dissolve liposomes. In most cases, the time course of Cl^- release was fit to a single exponential with a leak term, as previously described[40]. However, for slow mutants the time course of efflux was better approximated by a linear fit, as the time constant became very large (>>100 s). In these cases efflux was fit to $Cl(t) = Cl(0) + (v + v_L) \times t$ where Cl(t) is the chloride concentration at time t, v is the velocity of efflux mediated by CLC-ec1 and v_L is the velocity of the leak, which was experimentally determined from six or more independent sets of protein-free liposomes $v_L = 1.24 \pm 0.27 \times 10^{-3}$ nmol $Cl^- s^{-1}$. The turnover rate, γ, was calculated from the velocity as described[40]. As expected, for fast mutants the two approaches gave a comparable estimate of γ.

Crystallization. The A399C A432C mutant of CLC-ec1 was crystallized as a complex with a Fab fragment, as previously described[12,39]. Briefly, protein was incubated with a three-fold excess of Fab fragment and then purified over gel filtration preequilibrated in buffer B with 50 μM DMNG. The complex, concentrated to 5–12 mg/mL, was mixed with an equal volume of 100 mM NaCl, 20–30% (w/v) PEG 400, 50 mM ADA, pH 6.5, HEPES, pH 7.5, and Tris, pH 8.5. Crystals grew by vapor diffusion in sitting-drop trays for 2–10 weeks at 20 °C and were directly harvested from the drop, flash frozen and stored in liquid N_2. Diffraction data were collected to 3.5 Å at the X25 beamline (Brookhaven NSLS) and were processed by HKL2000 (**Table 2**). Phases were obtained by molecular replacement with the WT protein in complex with Fab (PDB 1OTS)[12] as the search model with ions, waters, and CLC-ec1 residues 397–401 and 429–434 removed[12,58]. Refinement was done by Phenix with initial rigid-body refinement and several subsequent rounds of minimization rebuilding the region of the Cys399 and Cys432 cross-link[59].

Binding measurements with isothermal titration calorimetry. Cl^- binding to the A399C A432C mutant of CLC-ec1 was carried out as described[36,38] with a nanoITC instrument (TA Instruments). For these experiments, in a final purification step, the protein was purified over a gel-filtration column preequilibrated in 100 mM potassium sodium tartrate, 20 mM HEPES, 50 μM DMNG, pH 7.5 (buffer B_0), and concentrated to 50–195 μM. The A399C A432C mutant was not stable in the absence of Cl^- upon incubation with Hg^{2+}. Therefore, in this case, the Hg^{2+} reaction was carried out in buffer B. Excess Cl^- and Hg^{2+} were successively removed by running the protein over a gel-filtration column preequilibrated in buffer B_0. The injection syringe was filled with buffer B_0 with 50 mM KCl added, to achieve final molar ratios of 100–250. Each experiment consisted of 30–48 injections of 1 μl of the ligand solution at 3–4 min intervals into the experimental chamber kept under constant stirring at 350 r.p.m. and at 25.0 ± 0.1 °C. All solutions were filtered and degassed before use. The ITC data were fit to a single-site Wiseman isotherm as described[36,38] with the NanoAnalyze program from TA instruments.

Cl^-/Cl^- exchange. Cl^- uptake measurements were carried out as previously described[57,60]. The averaged time course was fit to a saturating single exponential function of the form $C(t) = a_M \times (1 - \exp(-t/\tau))$ for A399C A432C and to a line $C(t) = a_0 + Kt$ for A399C $A432C_{Hg}$. The initial rate of uptake, K, was calculated as a_M/τ for A399C A432C and determined from the fit for A399C $A432C_{Hg}$.

Mutagenesis. All mutagenesis was carried out with the QuikChange method (Stratagene) and the mutated genes fully sequenced.

57. Accardi, A., Kolmakova-Partensky, L., Williams, C. & Miller, C. Ionic currents mediated by a prokaryotic homologue of CLC Cl^- channels. *J. Gen. Physiol.* **123**, 109–119 (2004).
58. McCoy, A.J. *et al.* Phaser crystallographic software. *J. Appl. Crystallogr.* **40**, 658–674 (2007).
59. Adams, P.D. *et al.* PHENIX: a comprehensive Python-based system for macromolecular structure solution. *Acta Crystallogr. D Biol. Crystallogr.* **66**, 213–221 (2010).
60. Maduke, M., Pheasant, D.J. & Miller, C. High-level expression, functional reconstitution, and quaternary structure of a prokaryotic ClC-type chloride channel. *J. Gen. Physiol.* **114**, 713–722 (1999).

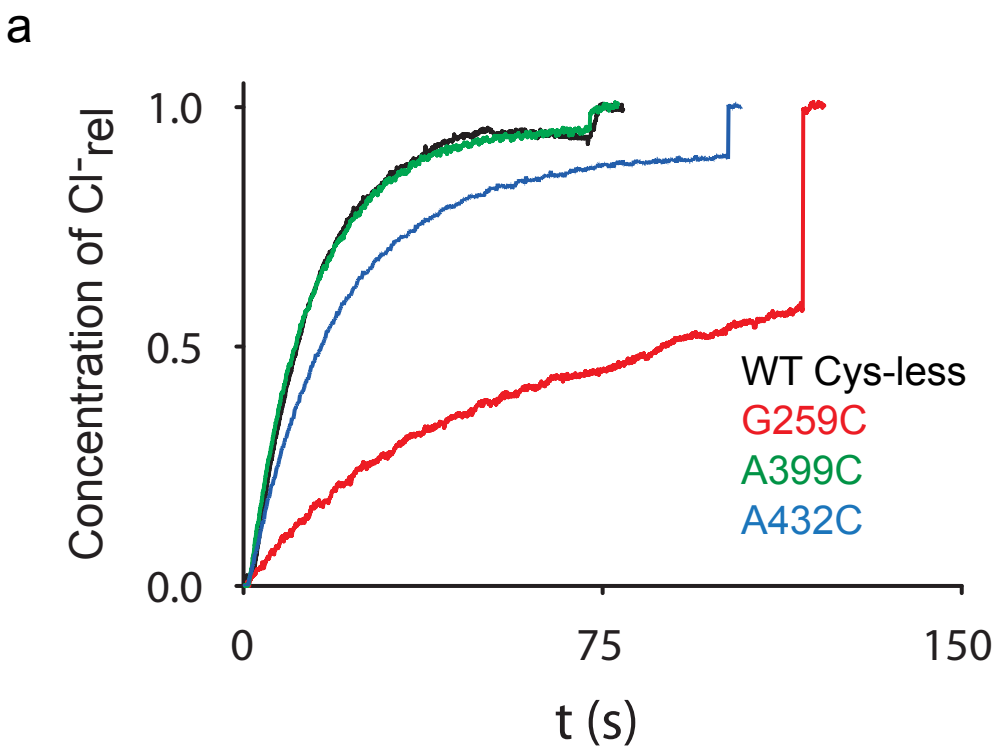

Supplementary Figure 1. Effect of single cysteine mutants on Cl^- transport. Representative traces of Cl^- efflux mediated by WT CLC-ec1 (black), G259C (red), A399C (green) and A432C (yellow) mutants of CLC-ec1. Averaged values of the Cl^- transport rates are reported in Table 1.

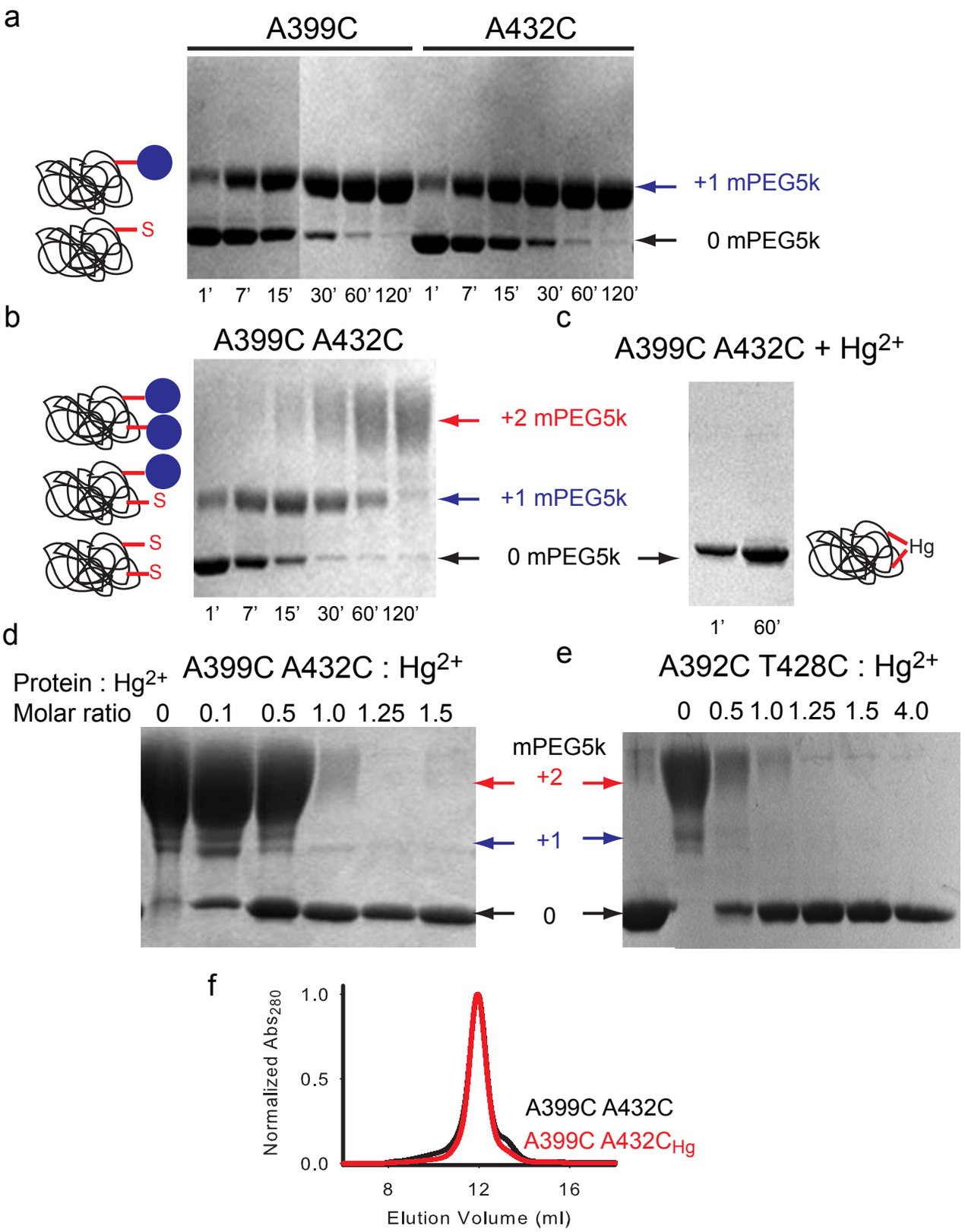

Supplementary Figure 2. Gel shift assay to determine the number of free cysteines. a-c) Time courses of reaction of the A399C and A432C single mutants (a), the A399C A432C double mutant before (b) and after (c) incubation with 30 μM Hg^{2+} for 60 min with 400 μM mPEG5K. Arrows denote the positions of the un-reacted and singly or doubly reacted proteins. Arrows indicate the positions of the protein when unreacted (black), singly (blue) or doubly reacted (red). d-e) Titration of Hg-induced protection from PEG-ylation of the strongly inhibited mutant A399C A432C (d) and of the non-inhibited mutant A392C T428C (e). f) Gel filtration profiles of the A399C A432C mutant before (black) and after (red) incubation with Hg^{2+}.

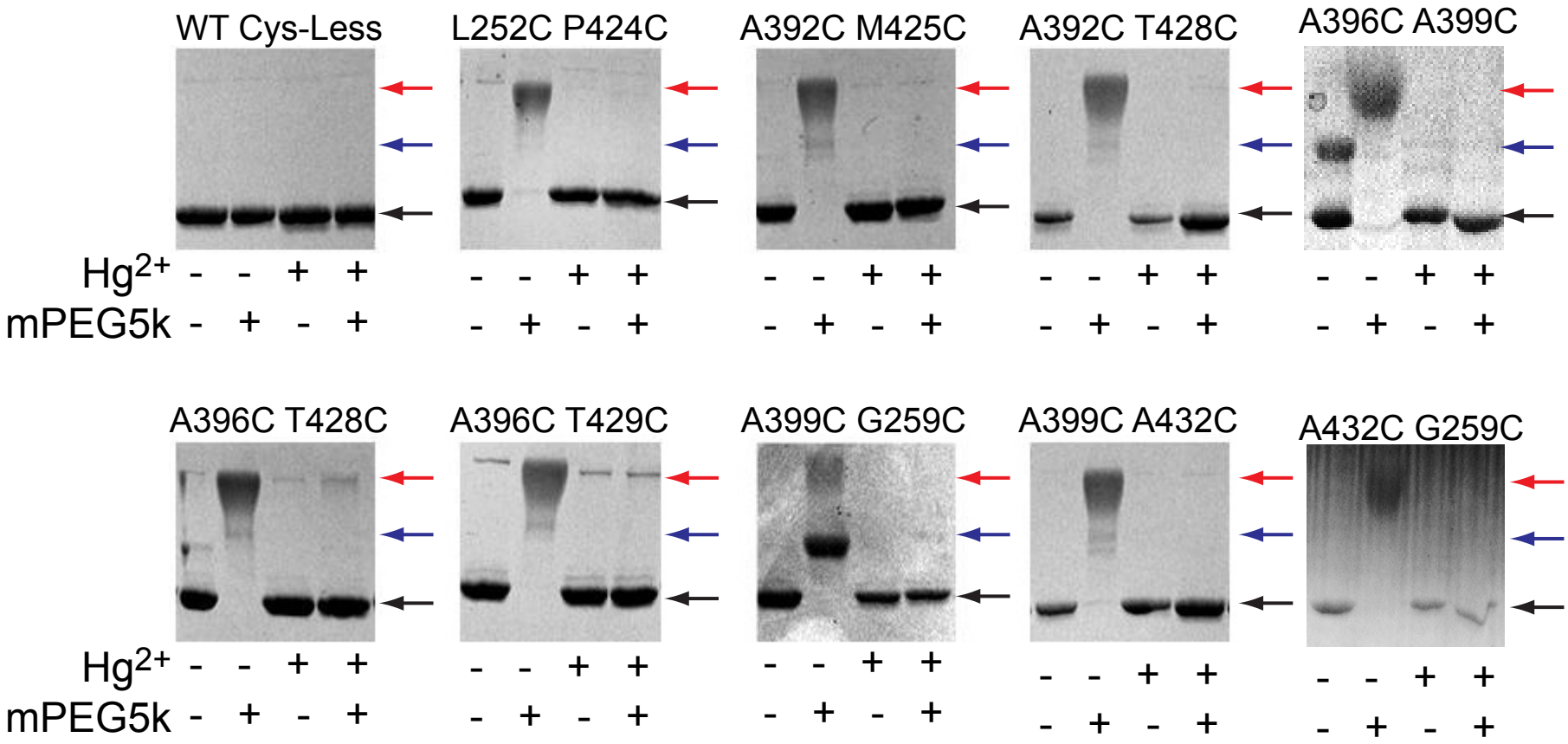

Supplementary Figure 3. Hg^{2+} treatment completely protects the 9 double mutants from PEG-ylation. The proteins were incubated with 200 μM Hg^{2+} for 60 min prior to a 120 min incubation with 1 mM mPEG5K. Arrows denote the position of the unreacted (black), singly (blue) or doubly reacted (red) proteins as in Supplementary Figure 2.

Nature Structural and Molecular Biology: doi:10.1038/nsmb.2814

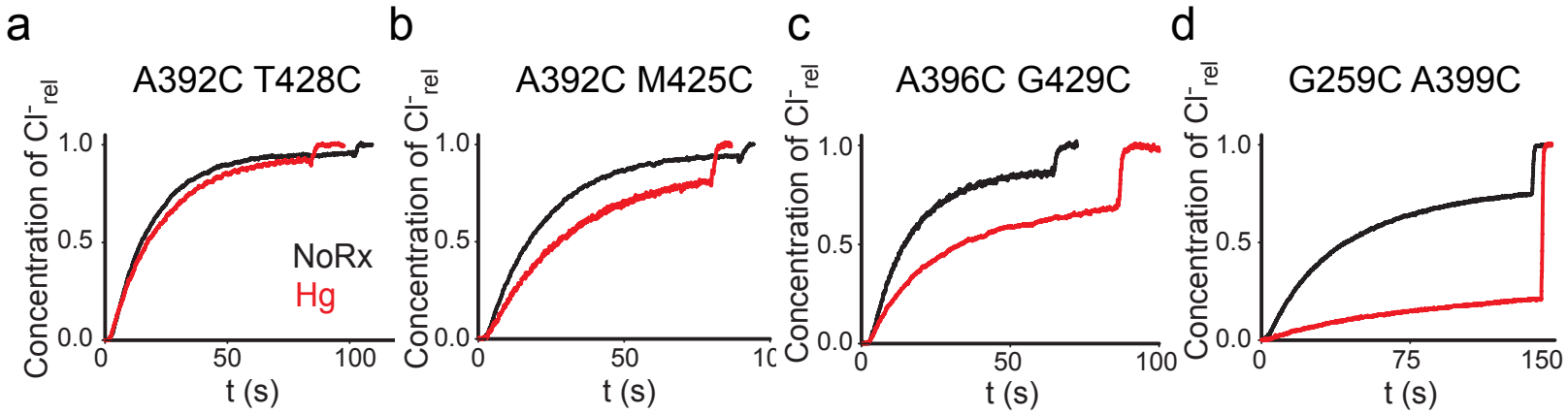

Supplementary Figure 4. Effect of crosslinks at additional positions. a -d) representative traces of Cl^- efflux mediated by the A392C T428C (a), L252C P424C (b), A396C G429C (c) and G259C A399C (d) mutants of CLC-ec1 before (black) and after (red) crosslink formation. Average±s.e.m. of the Cl^- transport rates are reported in Table 1.

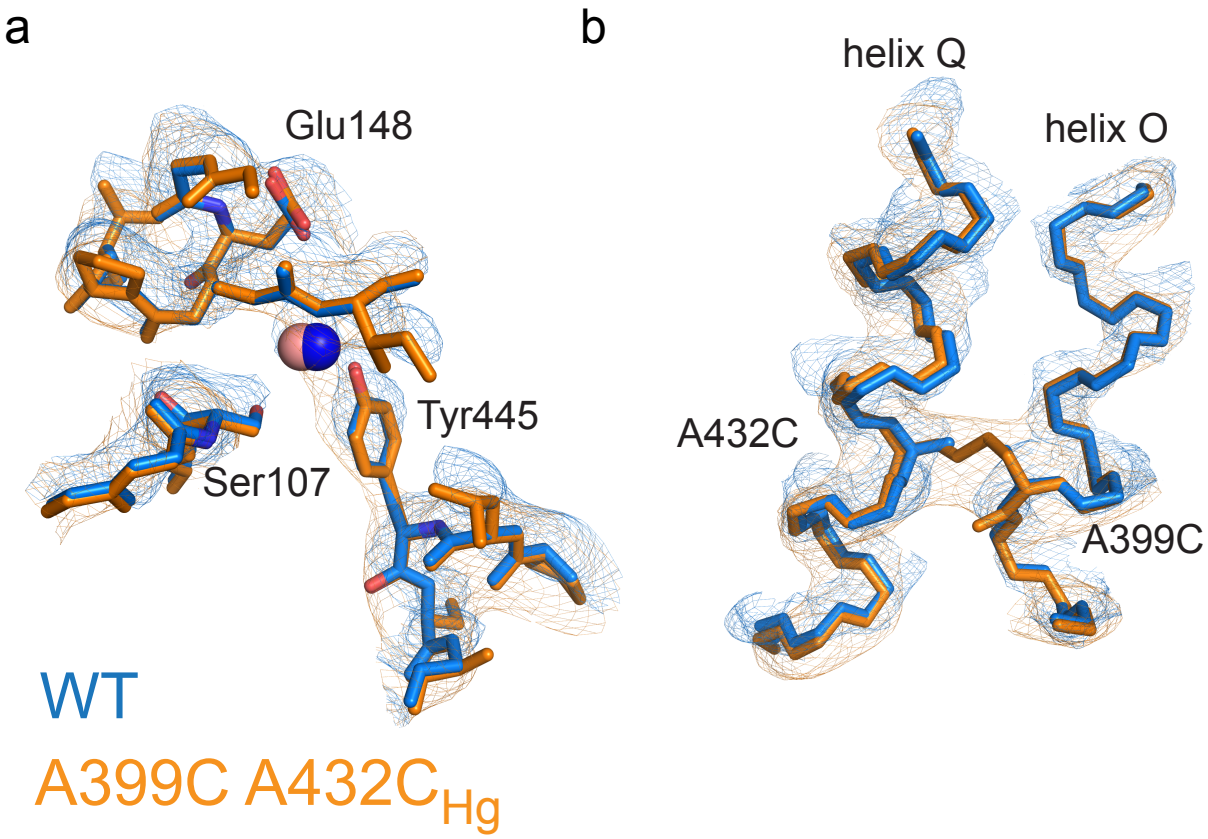

Supplementary Figure 5. Structural alignment of WT and A399C A432C$_{Hg}$ CLC-ec1. Alignment of the structures of WT (PDBID: 1OTS, blue) and A399C A432C$_{Hg}$ (PDBID: 4MQX, orange) in the ion binding region (a) and of helices O and Q around the crosslink region (b). Electron densities are contoured at 1σ and the Cl^- ions are represented as blue (WT) and salmon (A399C A432C$_{Hg}$) colored spheres.

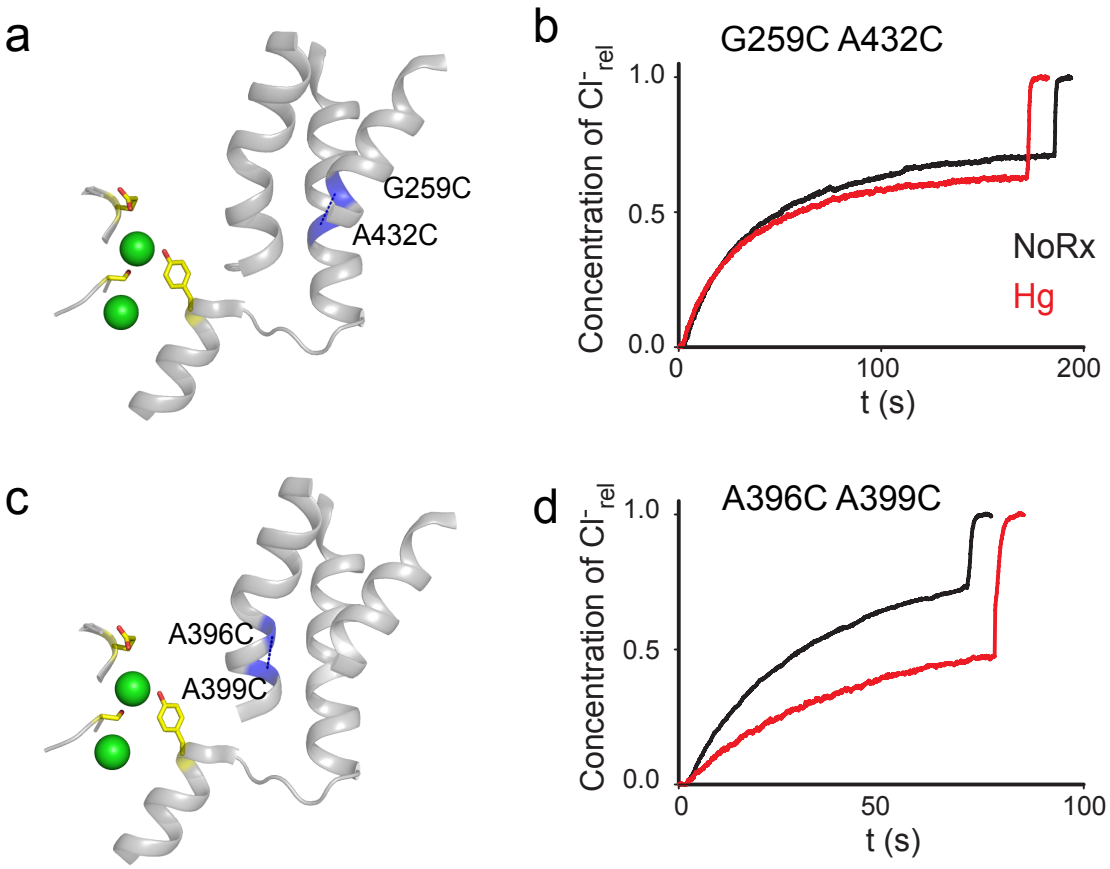

Supplementary Figure 6. Helix O moves relative to helices J and Q. a, c) Location of the crosslink between helices J and Q (A432C G259C) (a) and of the intrahelix crosslink in helix O (A396C A399C) (c). b, d) Functional effect of crosslinks at G259C A432C (b) and A396C A399C (d) before (black) and after incubation with Hg^{2+} (red). Means, errors and number of repeats of the transport rates are reported in Table 1.

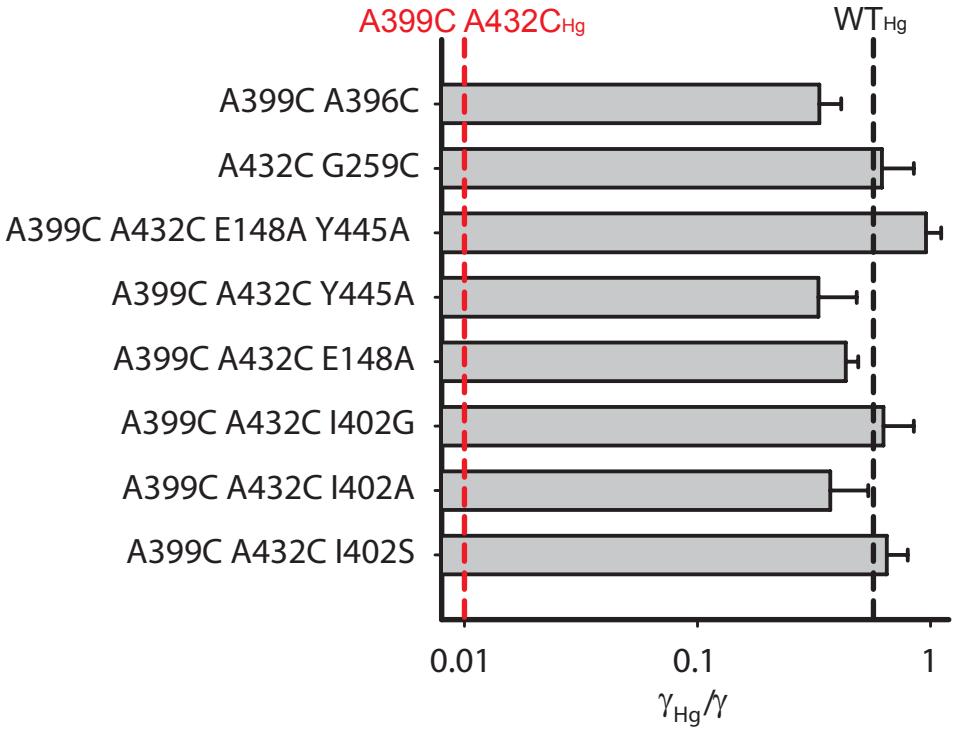

Supplementary Figure 7. The A399C A432C crosslink acts on the Cl^- pathway. Averaged reduction of the transport rate induced by Hg^{2+}- treatment for the indicated mutants. For reference the reduction of the WT Cys-less CLC-ec1 (black) and A399C A432C$_{Hg}$ (red) are shown as dashed lines.

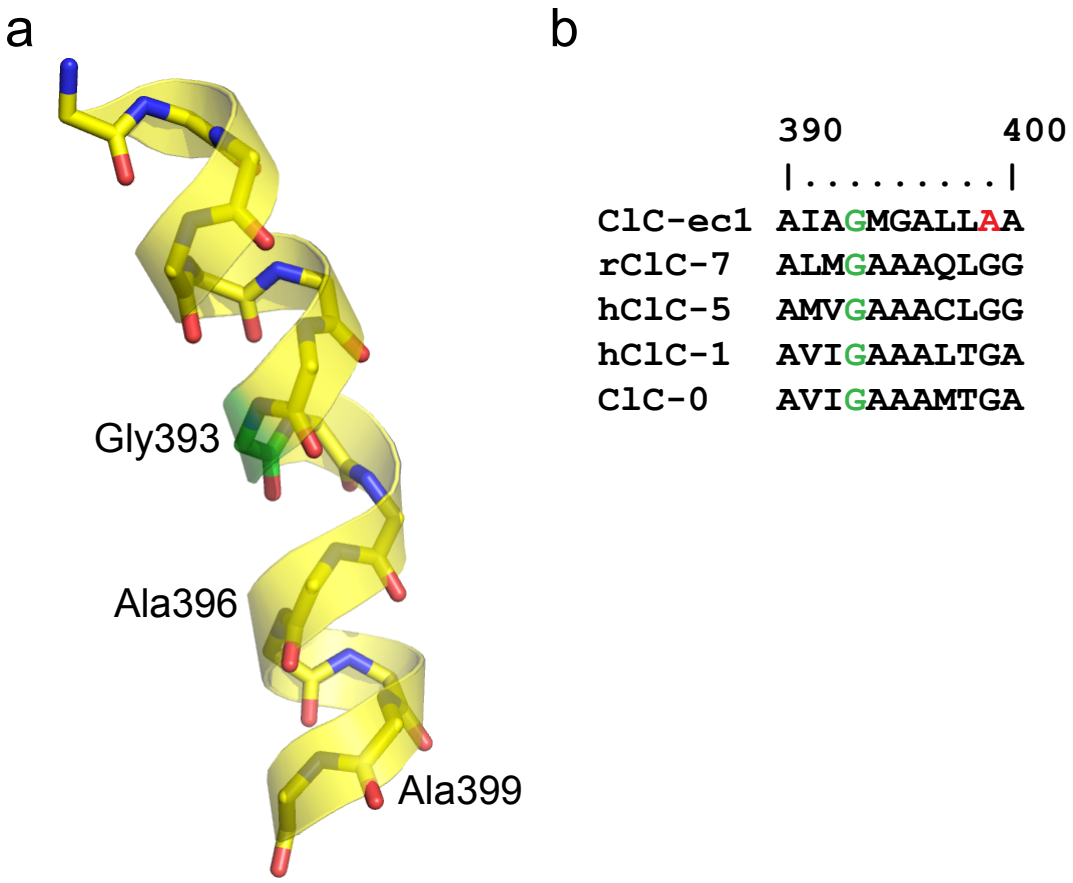

Supplementary Figure 8. Helix O is kinked at G393. a) Ribbon representation of helix O. For clarity the backbone atoms are also shown. Gly393 is colored in green. b) Alignment of the residues comprising the central portion of helix O from CLC-ec1, rCLC-7, hCLC-5, hCLC-1 and CLC-0. Gly393 is highlighted in green and Ala399 is shown in red.

	ΔH **(kcal mol^{-1})**	**TΔS** **(kcal mol^{-1})**	**ΔG** **(kcal mol^{-1})**	**K_d** **(μM)**	**# exp**
A399C A432C	-6.64±0.41	2.49±0.40	-4.16±.002	903±30	3
A399C A432C$_{Hg}$	-8.89±0.94	5.47±0.96	-3.43±0.09	3238±481	5

Supplementary Table 1. Thermodynamic parameters for Cl^- binding to the A399C A432C mutant of CLC-ec1 before and after crosslink formation. K_d and ΔH were obtained from a fit to a single site binding isotherm, while ΔG and TΔS were calculated from $\Delta G = RT \ln K_d$ and $T\Delta S = \Delta H - \Delta G$. Data is the mean±s.e.m. of the indicated number of experiments.